Electroless Deposition and Characterization of Pt_xRu_{1-x} Catalysts on Pt/C Nanoparticles for Methanol Oxidation

William E. Mustain
Department of Chemical, Materials, and Biomolecular Engineering,
University of Connecticut,
Storrs, CT 06268

Hyea Kim

Vijai Narayanan

Tyler Osborn

Paul A. Kohl
e-mail: kohl@gatech.edu

School of Chemical and Biomolecular Engineering,
Georgia Institute of Technology,
Atlanta, GA 30332

The electroless deposition of Pt_xRu_{1-x} catalysts using hydrazine dihydrochloride or formic acid as the reducing agent in a modified Leaman bath was investigated. The effect of potential on the Pt_xRu_{1-x} composition was investigated by potentiostatically depositing Pt_xRu_{1-x} thin films on gold from acidic chloride electrolytes at potentials between −0.46 V and 0.34 V (versus normal hydrogen electrode). The physical characteristics and elemental composition of the deposits were determined. An empirical model for the deposition process was developed, taking into account reactant concentration, temperature, and surface potential. The model accurately characterized the deposit composition over a wide Pt/Ru range. The surface potential was estimated to be 0.15 V during electroless deposition using formic acid as the reducing agent based on the empirical model. Deviations from the model were found when hydrazine was used as the reducing agent due to the formation of solution phase ruthenium complexes with hydrazine.
[DOI: 10.1115/1.4000675]

Keywords: platinum, ruthenium, deposition, fuel cell, methanol

1 Introduction

Direct methanol fuel cells (DMFCs) can have high energy density if concentrated methanol can be used as the fuel. They are potentially useful as a compact power source if the balance of plant can be minimized. Miniature DMFCs operating at low power require simple delivery of fuel to the anode electrode, efficient release of carbon dioxide products from the fuel container, and low methanol permeability through the proton-conducting electrolyte [1,2].

Several polymeric [2–5] and organic/inorganic hybrid membranes [2,6,7] have been investigated in order to lower the methanol permeability of the DMFC membrane. Unfortunately, even though the best-performing membranes have significant methanol permeability for low power devices. Methanol crossover is facilitated by high free volume and high water uptake in the membrane, which is needed for ion transport. The large free volume allows for facile methanol transport via diffusion and electro-osmotic drag during operation.

Silicate glass membranes have been developed as proton-conducting electrolytes for DMFCs in an effort to lower methanol permeability. Silicate electrolytes have been prepared by plasma enhanced chemical vapor deposition (PECVD) and sol-gel routes. PECVD membranes are typically prepared as thin films using silane and nitrous oxide as the reaction precursors [1,8,9]. It was found that PECVD glass materials provide proton conductivity through defect sites in the glass. The proton conductivity can be increased by controlling the deposition conditions. However, PECVD glasses are brittle and tend to have limited conductivity. Sol-gel synthesis provides considerable flexibility in the chemical structure and mechanical properties because many silicon-containing precursors are available. Sol-gel derived glasses can be engineered to provide higher conductivity and mechanical strength than PECVD glasses [10,11]. The permeability coefficient for methanol through silica glasses can be as much as four orders of magnitude lower than through Nafion [12,13]. The permeability improvement caused the ionic conductivity to also decrease, although by a smaller amount (approximately about two orders of magnitude). Silicate-based electrolytes prepared through sol-gel synthesis are a candidate for low crossover proton-conducting membranes in micro DMFCs.

Nafion-based DMFCs generally use catalyst layers containing Nafion for both the anode and cathode in order to construct a membrane electrode assembly (MEA). The presence of Nafion in the catalyst layer poses several problems, including chemical stability of the Nafion solution in the electrode in the liquid-fuel compartment and degradation of the cathode at low relative humidity. When a silica membrane is used in the MEA, there is a mismatch in thermal expansion coefficient between the electrode layer and glass electrolyte, which could lead to delamination and electrode failure. Recently, a sol-gel based carbon-supported platinum $(Pt/C)-SiO_2$ glass composite catalyst was used in the micro DMFC [14]. Here, the Pt/C nanoparticles were incorporated into a porous, sol-gel based SiO_2. The sol-gel matrix was made through the hydrolysis and condensation of tetraethyl orthosilicate (TEOS). This resulted in a glass layer impregnated with catalyst. However, the resistivity was high (5000 Ω cm) due to the fine dispersion of the Pt/C particles. Higher Pt/C loading would have resulted in lower sheet resistivity, but at the expense of mechanical strength and stability. Additional platinum was added to the electrode by electroless plating of platinum on the exposed Pt/C particles. Thus, the original Pt/C particles served to anchor metal in the TEOS-based glass and any amount of additional platinum could be added to the surface, giving the desiredresistivity (<100 Ω cm) The glass-based MEA also served to decrease the permeability of methanol through the membrane, as compared with a Nafion-based MEA.

A platinum-only electrode suffers from carbon monoxide poisoning in DMFC cells. CO strongly binds to platinum and interferes with further oxidation, yielding carbon dioxide [15]. The bifunctional mechanism is the preferred route to methanol oxidation to carbon dioxide, where the platinum is used with a more oxyphilic material, such as ruthenium, mitigating carbon monox-

Manuscript received December 8, 2008; final manuscript received July 23, 2009; published online April 8, 2010. Editor: Nigel M. Sammes.

ide poisoning [16]. The 1:1 Pt-to-Ru ratio is preferred for methanol oxidation catalysts [17]. Since the current density, and thus power density of the DMFC, is a strong function of the anode catalyst, it is important to achieve high electrochemical activity. In the case of TEOS sol-gel electrode with imbedded Pt/C catalyst, this requires the electroless deposition of a PtRu (1:1) catalysts layer.

In a previous publication, we described the electroless deposition of PtRu electrocatalysts for methanol oxidation using a Leaman bath with hydrazine as the reducing agent [18]. In that investigation, it was found that it was possible to deposit Pt_xRu_{1-x} over a wide range of compositions by changing the bath makeup and temperature; however, a $Pt_{0.5}Ru_{0.5}$ deposit was not obtained and the samples showed significant variance at high temperatures. In this report, the electro and electroless deposition of Pt_xRu_{1-x} electrocatalysts were further characterized. Additional electroless Pt_xRu_{1-x} electrodes were prepared in the Leaman bath using hydrazine dihydrochloride. Also, Pt_xRu_{1-x} deposits were prepared using formic acid as the reducing agent in the Leaman bath. Finally, an improved empirical relationship for deposit composition as a function of bath concentrations, temperature and surface potential compared with our previous work [18] is presented.

2 Experimental

The electrodeposition of the Pt_xRu_{1-x} catalysts was carried out on gold electrodes. The electrodes were immersed into an electrolyte, which contained 3 g/100 mL HCl (Sigma Aldrich, St. Louis, MO), 0.4 g/100 mL H_2PtCl_6 (Sigma Aldrich), and 0.1 g/100 mL $RuCl_3$ (Sigma Aldrich), which corresponds to a Pt-to-Ru mole ratio in solution of 1.6:1. The counterelectrode was a 1 mm diameter platinum wire (Sigma Aldrich). The reference electrode was $Hg/HgSO_4$ (Pine Instrument Co., Grove City, PA) (E^o=0.64 V versus a normal hydrogen electrode (NHE)) and all potentials are reported versus NHE. Chronoamperometric experiments were carried out at potentials between −1.1 V and −0.3 V (−0.46 V and 0.34 V versus NHE) with a PARSTAT 2263 Potentiostat.

The electroless deposition of the Pt_xRu_{1-x} films was carried out on carbon-supported platinum electrodes in a modified acidic Leaman bath [19,20]. The preparation of the $Pt/C-SiO_2$ electrodes has been described previously [14]. The aqueous electroless bath contained 3.0 g/100 mL HCl, 0.2 g/100 mL 5-sulfosalycylic acid hydrate (Sigma Aldrich), 0.05 g/100 mL 1,3,6-sodium naphthalene trisulfonate tribasic hydrate (Sigma Aldrich), and 0.06 g/100 mL benzene 1,3-disulfonate (Sigma Aldrich). The reducing agent was either hydrazine dihydrochloride or formic acid (1 g/100 mL). Hexachloroplatinic acid and ruthenium (III) chloride were used as the source of Pt and Ru ions, respectively.

The composition of the deposited Pt_xRu_{1-x} films was estimated using a Zeiss Ultra 60 scanning electron micrograph with energy dispersive X-ray (EDX) analysis. The primary electron energy for the analysis was 15 keV.

3 Empirical Model for Pt_xRu_{1-x} Electrodeposition

The standard reduction potential for platinum and ruthenium chloride are separated by 0.33 V with platinum, which is a more noble metal (see Eqs. (1) and (2), respectively) [21]

$$PtCl_6^{-2} + 4e^- \rightarrow Pt(s) + 6Cl^-, \quad E^o = 0.73 \text{ V} \tag{1}$$

$$RuCl_5^{-2} + 3e^- \rightarrow Ru(s) + 5Cl^-, \quad E^o = 0.4 \text{ V} \tag{2}$$

Thus, the deposition of platinum is favored at potentials near their standard potentials. At potentials sufficiently negative of their standard potentials, mass transfer is expected to limit the deposition rate of each metal. In this development, the relationship between current and overpotential ($E-E^o$) is given by the Butler–Volmer kinetic expression (Eq. (3))

$$N_j = \frac{i_j}{n_j \mathrm{F}} = A k_j C_j \exp\left[\frac{\mathrm{F}\alpha_j}{RT}(E - E_j^o)\right] \tag{3}$$

where N_j is the number of moles of either Pt or Ru deposited, i_j is the current associated with the deposition of either Pt or Ru, n is the number of equivalents per mole, F is Faraday's constant, A is the electrode area, k_j is the electrochemical rate constant, C_j is the bulk concentration of the species j, α_j is the effective transfer coefficient for each reduction process, R is the ideal gas constant, and T is the absolute temperature. It is recognized that the standard potential for the combined deposition of the two metals may differ from the pure metal's standard potential.

The percentage of ruthenium in the deposit X can be expressed in terms of the reduction current going to each ion $PtCl_6^{-2}$ and $RuCl_5^{-2}$ (Eq. (4))

$$X = 100\left(\frac{N_{\mathrm{Ru}}}{N_{\mathrm{Pt}} + N_{\mathrm{Ru}}}\right) = 100\left(\frac{1}{\frac{N_{\mathrm{Pt}}}{N_{\mathrm{Ru}}} + 1}\right) \tag{4}$$

The relative reaction rate for the two species ($i_{\mathrm{Pt}}/i_{\mathrm{Ru}}$) can be found by first applying Eq. (3) to both species and dividing them, yielding Eq. (5)

$$\frac{N_{\mathrm{Pt}}}{N_{\mathrm{Ru}}} = \frac{A k_{\mathrm{Pt}} C_{\mathrm{Pt}} \exp\left[\frac{\mathrm{F}\alpha_{\mathrm{Pt}}}{RT}(E - E_{\mathrm{Pt}}^o)\right]}{A k_{\mathrm{Ru}} C_{\mathrm{Ru}} \exp\left[\frac{\mathrm{F}\alpha_{\mathrm{Pt}}}{RT}(E - E_{\mathrm{Ru}}^o)\right]} \tag{5}$$

This exponential terms can be merged and expanded

$$\frac{N_{\mathrm{Pt}}}{N_{\mathrm{Ru}}} = \frac{k_{\mathrm{Pt}} C_{\mathrm{Pt}}}{k_{\mathrm{Ru}} C_{\mathrm{Ru}}} \exp\left[\frac{\mathrm{F}E}{RT}(\alpha_{\mathrm{Pt}} - \alpha_{\mathrm{Ru}}) + \frac{\mathrm{F}}{RT}(\alpha_{\mathrm{Pt}} E_{\mathrm{Pt}}^o - \alpha_{\mathrm{Ru}} E_{\mathrm{Ru}}^o)\right] \tag{6}$$

The constant terms in Eq. (6) can be combined to give two parameters a and b

$$\frac{N_{\mathrm{Pt}}}{N_{\mathrm{Ru}}} = a\left(\frac{C_{\mathrm{Pt}}}{C_{\mathrm{Ru}}}\right)\exp\left[\frac{b}{T}E\right] \tag{7}$$

where

$$a = \frac{k_{\mathrm{Pt}}}{k_{\mathrm{Ru}}} \exp\left[\frac{\mathrm{F}}{RT}(\alpha_{\mathrm{Pt}} E_{\mathrm{Pt}}^o - \alpha_{\mathrm{Ru}} E_{\mathrm{Ru}}^o)\right] \tag{8}$$

and

$$b = \frac{\mathrm{F}}{R}(\alpha_{\mathrm{Pt}} - \alpha_{\mathrm{Ru}}) \tag{9}$$

where b is a temperature independent constant and the inverse of the Tafel slope. Rearranging Eq. (7) yields a simple expression for the relative deposition rates of Pt and Ru

$$\ln\left(\frac{N_{\mathrm{Pt}}}{N_{\mathrm{Ru}}}\right) = \ln\left(a\left[\frac{C_{\mathrm{Pt}}}{C_{\mathrm{Ru}}}\right]\right) + \frac{b}{T}E \tag{10}$$

The parameter a has a convoluted temperature dependence. This approach requires that the heterogenous rate constant and transfer coefficient for each metals on the surface remain essentially constant with Pt_xRu_{1-x} composition. The rate constant data are contained in parameter a as well as the thermodynamic effects E_j^o for the metals. Accurate determination of a is needed in order to reliably describe the deposition process.

4 Results and Discussion

Gold electrodes were immersed in the plating solution with a Pt^{+4}/Ru^{+3} ion ratio of 1.6 at various working potentials between −0.46 V and 0.34 V at 23 °C. This was done in order to determine the effect of surface potential on the deposit composition. The plots showed typical behavior for metal deposition, where the

Table 1 Electrodeposit composition and relative reduction rate as a function of electrode potential at 23°C and $C_{Pt}/C_{Ru}=1.6$

Potential (E)	Ru content (%)	i_{Pt}/i_{Ru}
−0.46	44	1.3
−0.26	38	1.6
−0.06	28	2.6
0.04	37.5	1.7
0.14	28	2.6
0.24	8.0	11
0.29	3.5	27
0.32	4.0	24
0.34	2.3	43

current initially decays during the buildup of the concentration gradient before quickly leveling off to give a steady state current. The stability of the steady current indicated that the electrode surface area does not significantly change during the deposition, which points to a smooth, low surface roughness deposit. Also, it should be noted that the observed current at lower potentials was significantly increased compared with higher surface potentials [18]. This is consistent with Eq. (3), where the increased driving force for the deposition at the more cathodic electrode potential is expected to increase the reaction rate.

The composition of the electroplated Pt_xRu_{1-x} deposits was determined by EDX. Following the surface characterization, Eq. (4) was used to determine the relative deposition rates for Pt and Ru. Several samples were prepared at each potential. Table 1 shows the Pt_xRu_{1-x} electrodeposit composition as a function of electrode potential. It can be seen that the ruthenium content in the deposit increases with decreasing electrode potential, which is consistent with expectations.

In order to determine the deposition parameters a and b at room temperature (23°C) $\ln(i_{Pt}/i_{Ru})$ was plotted as a function of the electrode potential. As expected, the relationship between the two is linear, which indicates that the derived relationship is valid. However, two different linear regimes are observed [18]. The first occurs at higher electrode potentials (above 0.1 V). The second appears to be applicable at potentials below 0.1 V. There are two possible explanations for the appearance of a secondary region. First, an interfering reaction may be present. In this case, the hydrogen evolution reaction is most likely as the adsorption and reduction in hydrogen ions from the acidic solution on certain crystal faces of Pt begins at around 0.2 V and reduces efficiently on all surfaces in acidic solutions near 0.0 V. The second possibility is a change in the rate-limiting step in the reaction. Second, at large reaction overpotentials, the mass transport resistance plays an increasing role in the process and may explain the deviation here. Therefore, the composition data between 0.1 V and 0.35 V versus NHE was used to determine a and b in the empirical model, which is presented in Fig. 1.

Linear regression for the linear region between 0.1 V and 0.35 V in Fig. 1 yields a and b values of 0.247 and 4080, respectively. The value for a suggests that the electrochemical rate constant for the two components are comparable, although ruthenium is likely a bit higher. This seems reasonable, considering the number of electron transfer steps and relative size of the two metal ions. The value for b also appears to fall within an acceptable range at 23°C, yielding a combined Tafel slope value of 167 mV/decade.

Pt_xRu_{1-x} deposits were prepared at 23°C, 50°C, 70°C, and 90°C with a Pt/Ru ratio of 1.6 in the deposition bath in order to determine a as a function of temperature. The Ru content of the resulting electrodeposits were 1.0%, 1.5%, 1.8%, and 2.1%, respectively. Since b is temperature independent, Eq. (10) can be used to calculate a as a function of temperature. The calculated values for a were 0.262, 0.292, and 0.324 at 50°C, 70°C, and 90°C, respectively. This indicates that the platinum ion kinetics improve relative to ruthenium at higher temperature. However, determining the exact cause of the improvement is difficult since a is a very complicated function of the temperature. The kinetic rate constant changes as an Arrhenius function, where the activation energies are unknown. Also, the thermodynamic potential for the deposition processes will change as a function of temperature in accordance with the Nernst equation.

The electroless metal deposition process occurs through a surface-catalyzed galvanic reaction between the metal ions and the reducing agent. The reductant and oxidant electrochemically react on active surface sites. The oxidation and reduction reactions can occur at different sites. Since the distance between active sites and the resistance of the conductive substrate are negligibly small, the surface potential is essentially constant and the reduction and oxidation occur at a single potential, often called the mixed potential. The resulting mixed potential is between the equilibrium potential of the oxidant and reductant such that the oxidation and reduction currents are equal.

Hydrazine was used as a reducing agent in the electroless process in order to assess the possibility of using a typical Leaman

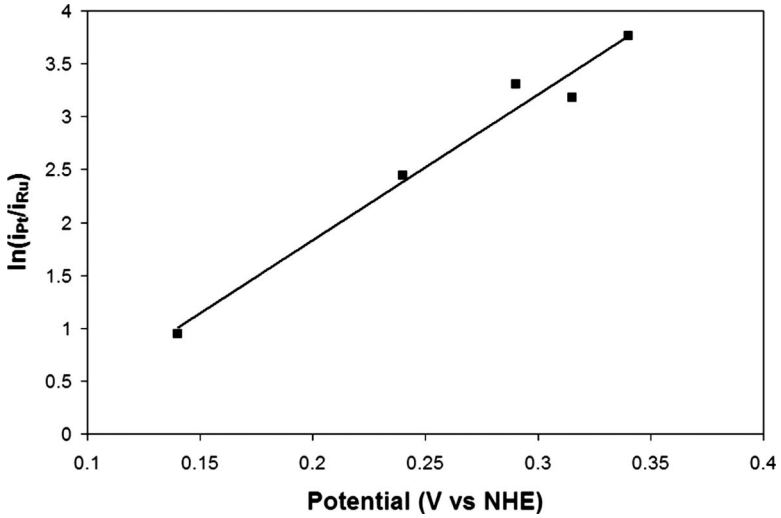

Fig. 1 Relative contributions to the observed current of Pt and Ru during electrodeposition as a function of potential at 23°C and $C_{Pt}/C_{Ru}=1.6$

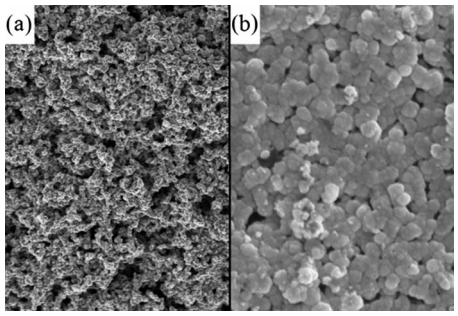

Fig. 2 Anode catalyst layer (*a*) before and (*b*) after the electroless deposition of PtRu at 11,000× and 60,000× magnifications, respectively

bath [21,22] to codeposit both Pt and Ru. The hydrazium ion is electrochemically active and its standard reduction potential is −0.23 V versus NHE [23]. The acid-base behavior and electrochemical oxidation are shown in Eqs. (11) and (12), respectively

$$N_2H_4 + H_3O^+ \rightarrow N_2H_5^+ + H_2O \tag{11}$$

$$N_2H_5^+ \rightarrow N_2 + 5H^+ + 4e^-, \quad E^o = -0.23 \text{ V} \tag{12}$$

Formic acid was also used as a reducing agent in the electroless process. The standard potential for formic acid oxidation is approximately −0.1 V versus NHE (Eq. (13))

$$HCOOH \rightarrow CO_2 + 2H^+ + 2e^-, \quad E^o = -0.1 \text{ V} \tag{13}$$

The standard potentials for hydrazine and formic acid are close to the lower end of the potential region of interest in Fig. 1. However, a significant overpotential for the oxidation of hydrazine and formic acid is expected. The overpotential during electroless deposition can be different from the overpotential of the pure reducing agent because of the changing nature of the surface being created. This overpotential forces the electroless deposition mixed potential positive of 0.1 V, making the parameters obtained from Fig. 1 usable.

Several $Pt/C-SiO_2$ composite catalyst layers were prepared on glass substrates according to our previously described procedure [14]. The composite electrodes are homogeneous and porous, as shown in Fig. 2(*a*). After 180 s, the particle size was 20–50 nm. The particle size increased from 50 nm to 100 nm after 300 s of deposition. Next, the electroless deposition of Pt_xRu_{1-x} electrocatalysts was carried out on the $Pt/C-SiO_2$ composite catalyst layers using the modified aqueous, acidic Leaman bath [21,22] with hydrazine as the reducing agent. The particle size was similar to that of the Pt/C layer.

In order to determine the electrode potential during the electroless process, several $Pt/C-SiO_2$ samples were immersed in the electroless bath at room temperature (23°C). Four different bath compositions were investigated, where the concentration of platinum and ruthenium ions in solution were adjusted such that their ratio (C_{Pt}/C_{Ru}) was equal to 1.6, 0.8, 0.4, and 0.2. A significant amount of metal was deposited on each sample, as shown in Fig. 2(*b*) (formic acid), in order to ensure a sample size large enough for accurate determination of the composition using EDX. Codeposition of metals often results in alloy formation, which is supported here by the uniformity and coexistence of Pt and Ru within the metal particles, as seen by EDX. When used as a fuel cell anode, the amount of deposited metal may be different than the amount deposited here and would need to be optimized for electrical conductivity, active area, and porosity [14].

The electrode potential in the empirical model was iteratively adjusted until an acceptable fit with metal composition was achieved. Here, the experimental data and empirical model agree well at approximately 0.40 V, as shown in Fig. 3. This is consistent with expectations, where the overpotentials for both the anodic and cathodic reactions incur a significant overpotential. It should be noted that the surface potential could not be directly measured during deposition due to the extremely low electrical conductivity of the $Pt/C-SiO_2$ electrolyte prior to reaching the percolation threshold, where a significant amount of material has already been deposited.

Unfortunately, even with a large excess of ruthenium ions in solution, the electroless deposition resulted in bimetallic layer with less than 8% Ru. Also, the empirical model suggests that C_{Pt}/C_{Ru} ratios of approximately 0.01 would be necessary to achieve equimolar deposition of the two metals and would be extremely sensitive to deviations in concentration. On the other hand, from the model parameters, it is expected that raising the

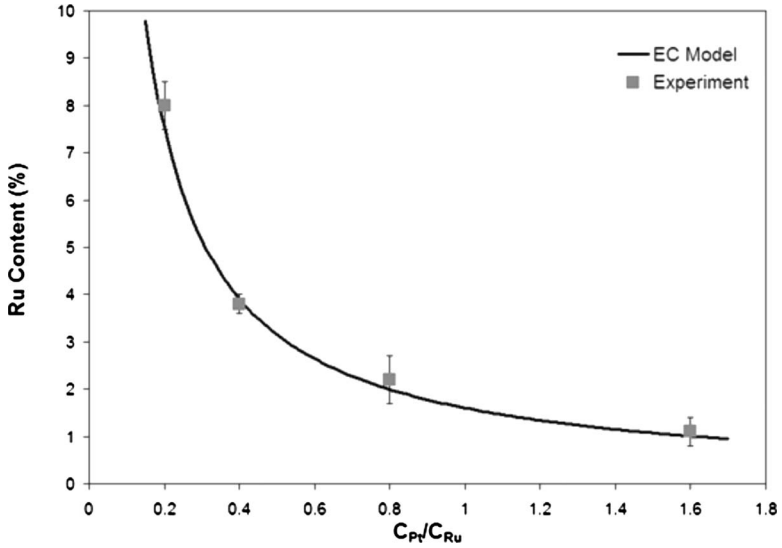

Fig. 3 Agreement between the proposed deposition model at a surface potential of 0.4 V and experimental data for the spontaneous, electroless deposition of Pt_xRu_{1-x} with a hydrazine dihydrochloride reducing agent at various bath compositions (23°C).

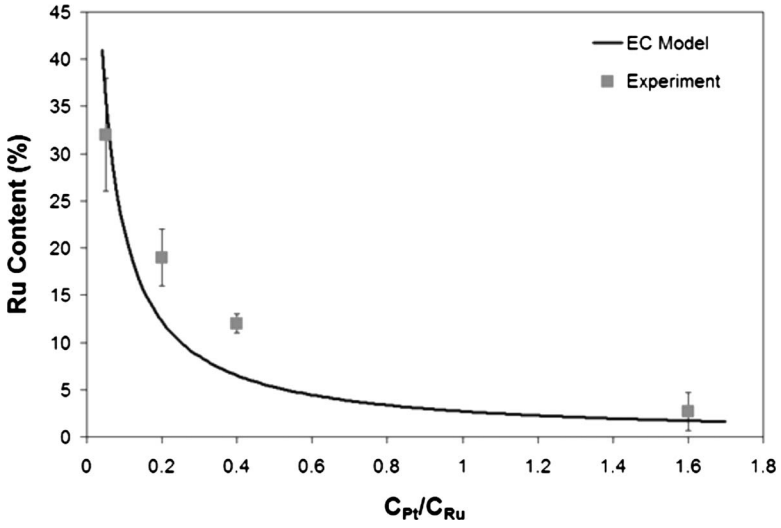

Fig. 4 Model and experimental results for the electroless deposition of Pt_xRu_{1-x} with hydrazine dihydrochloride reducing agent and various bath compositions (90°C)

temperature would provide a more controllable method by which to modify the deposit composition such that an optimum $Pt_{0.5}Ru_{0.5}$ could be obtained.

Pt_xRu_{1-x} was deposited at 90°C with a C_{Pt}/C_{Ru} ratio of 1.6, 0.4, 0.2, and 0.05. The resulting deposit compositions are shown in Fig. 4. The deposit composition deviates from the values expected from empirical model with a large variance in the composition of the deposit at low C_{Pt}/C_{Ru} ratios. Also, it should be noted that after several minutes in the electroless bath at 90°C, the metal layer showed poor adhesion.

Over only a few hours, the solution color turned from dark red, due to $RuCl_3$, to deep golden color. This is most likely due to the formation of a complex between ruthenium and hydrazine, which is favored at elevated temperatures. Specifically, $RuCl_3$ trihydrate readily reacts with hydrazine [23–25]

$$RuCl_3 \cdot 3H_2O \xrightarrow{N_2H_4} Ru(NH_3)_5N_2^{+2} \tag{14}$$

This species can further react in the presence of water (Eq. (15)) or chloride (Eq. (16))

$$Ru(NH_3)_5N_2^{+2} \xrightarrow{H_2O} Ru(NH_3)_5H_2O^{+2} \tag{15}$$

$$Ru(NH_3)_5N_2^{+2} \xrightarrow{Cl_2} Ru(NH_3)_6^{+2} \tag{16}$$

The formation of these ammoniacal species would significantly alter the deposition process, which was not accounted for in the model. The redox potential and kinetic parameters would be significantly different from the chloride complex.

Formic acid was investigated as a reducing agent for electroless deposition of PtRu due to its favorable oxidation potential, solubility, and electrochemical reactivity on Pt and PtRu surfaces [26]. Several $Pt/C-SiO_2$ composite electrodes were immersed in the electroless bath with formic acid as the reducing agent at 70°C. Several bath compositions were investigated with the C_{Pt}/C_{Ru} equal to 5.0, 1.0, 0.5, 0.67, and 0.2. This resulted in Pt_xRu_{1-x} deposits with a Ru content of 6.8%, 35%, 42%, 52%, and 75%, respectively. The ruthenium content of the electrodeposits was significantly higher when formic acid was used as the reducing agent instead of hydrazine, even though the Ru ion content in the bath and temperature were lower. The higher Ru content in the deposit suggests that the mixed potential during electroless deposition was more negative than with hydrazine. The mixed potential obtained from the empirical model developed in this study corresponds to approximately 0.15 V versus NHE during the deposition process.

The platinum-ruthenium bath using formic acid as the reducing agent appears stable with time. The composition of the deposit versus metal ratio in the bath is shown in Fig. 5. The wide range of values and close correlation to the model shows that the ruthenium ions are stable in the bath. The bath was also visually unchanged with time when aged at 70°C overnight.

The elemental distribution of platinum and ruthenium in the electrodeposit, as shown in Fig. 2(*b*), was examined using EDX elemental mapping. This is shown in Fig. 6 for a limited surface sampling. A uniform distribution of Pt and Ru were observed with no signs of metal segregation. This dispersion is verified by observing the electrodeposit with the SEM in both split in-lens and backscatter mode. Both are shown in Fig. 7. The backscatter SEM mode typically allows for qualitative assessment of the surface dispersion due to the differing emission of metals, where larger molecular weight materials are indicated by higher brightness intensity. Figure 7 shows no difference in intensity across the surface, which suggests that the surface is homogeneous and may be an alloy, though no additional characterization was performed to confirm this. A highly dispersed surface is critical for anode performance as an anode in a methanol fuel cell. Further investigation of the metal films as an anode in a methanol fuel cell is underway.

Finally, the electroless deposition of ruthenium without platinum was investigated. Experiments were carried out using hydrazine or formic acid as the oxidizing agent. EDX showed that only a very thin film of ruthenium was deposited. This leads to the conclusion that the catalytic surface for the reducing agent was platinum or the platinum-ruthenium catalyst surface. Once the Pt/C surface is covered with ruthenium, the electrode is rendered essentially inert and no additional Ru is deposited. When platinum is codeposited with ruthenium, the electrodeposit was several micrometers thick.

5 Summary

Pt_xRu_{1-x} bimetallic electrocatalysts for micro direct methanol fuel cells have been prepared by electroless deposition in an aqueous plating bath. The metal deposition process was consistent the behavior of a galvanic, electrocatalytic bath. An empirical electro-

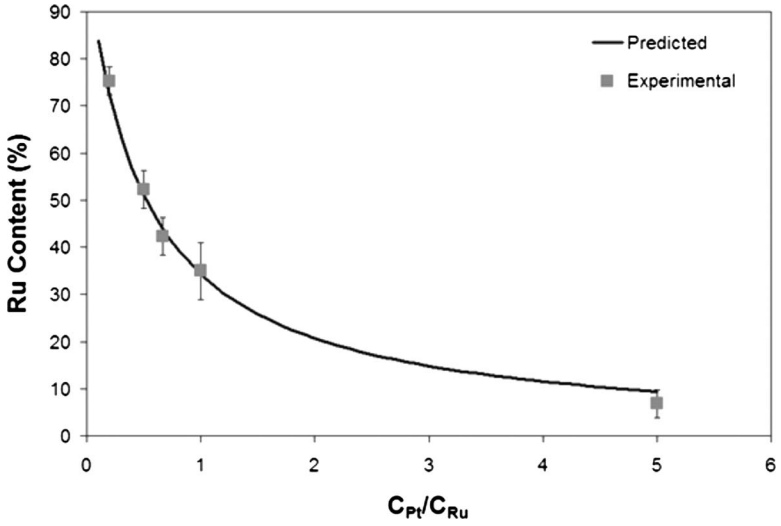

Fig. 5 Model and experimental results for the electroless deposition of Pt_xRu_{1-x} with formic acid reducing agent and various bath compositions (70°C)

chemical model was developed and the kinetic parameters were determined at temperatures between 23°C and 90°C. The model was found to be accurate over a wide range of temperatures and bath compositions. Ruthenium forms an ammoniacal complex when hydrazine was used as the reducing agent. Formic acid was found to be an improved reducing agent compared with hydrazine.

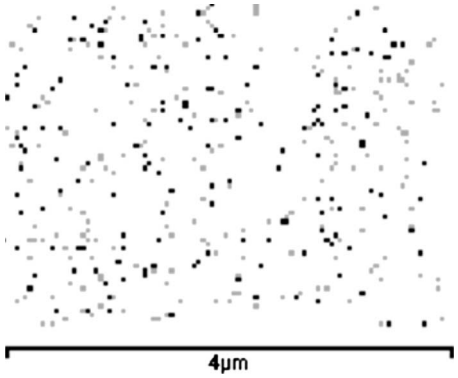

Fig. 6 EDX map for Pt (■) and Ru (□) in the $Pt_{0.48}Ru_{0.52}/C-SiO_2$ composite catalyst layer

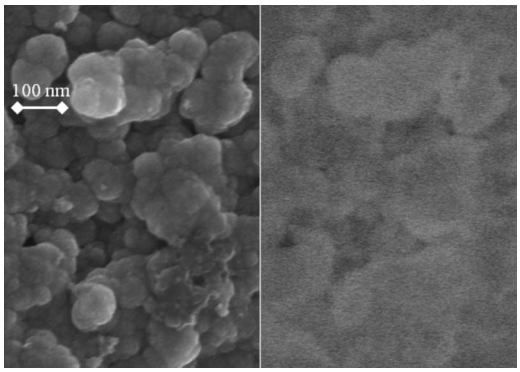

Fig. 7 SEM/backscatter SEM for PtRu catalyst layer, 125 k× magnification (100 nm marker shown)

Acknowledgment

This work is funded by the T&E/S&T Program through the Naval Undersea Warfare Center, Newport, RI, Contract No. N66604-06-C-2330.

Nomenclature

N_j = moles of species j reacted (mol/s)
i_j = current generated by reduction of species j (C/s)
n_j = stoichiometric number of electrons (mol e^-/mol j)
F = Faraday's constant (C/mol e^-)
A = electrode area (cm^2)
k_j = rate constant for reduction in species j (s^{-1})
C_j = concentration of species j in the bath (mol/cm^3)
α_j = transfer coefficient for reduction in j
R = ideal gas constant (J/mol K)
T = absolute temperature (K)
E = electrode potential (V)
E_j^{eq} = equilibrium potential for reduction of species j (V)
X = ruthenium content (%)
a = empirical rate constant
b = empirical Tafel slope

References

[1] Prakash, S., Mustain, W. E., Park, S., and Kohl, P. A., 2008, "Phosphorus-Doped Glass Proton Exchange Membranes for Low Temperature Direct Methanol Fuel Cells," J. Power Sources, **175**, pp. 91–97.
[2] DeLuca, N. W., and Elabd, Y. A., 2006, "Polymer Electrolyte Membranes for the Direct Methanol Fuel Cell: A Review," J. Polym. Sci., Part B: Polym. Phys., **44**, pp. 2201–2225.
[3] Rusanov, A. L., Likhatchev, D., Kostoglodov, P. V., Müllen, K., Klapper, M., and Schmidt, M., 2005, "Proton-Exchanging Electrolyte Membranes Based on Aromatic Condensation Polymers," Adv. Polym. Sci., **179**, pp. 83–134.
[4] Wang, Z., Li, X., Zhao, C., Ni, H., and Na, H., 2007, "Sulfonated Poly(ether ether sulfone) Copolymers for Proton Exchange Membrane Fuel Cells," J. Appl. Polym. Sci., **104**, pp. 1443–1450.
[5] Yang, B., and Manthiram, A., 2003, "Sulfonated Poly(ether ether ketone) Membranes for Direct Methanol Fuel Cells," Electrochem. Solid-State Lett., **6**, pp. A229–A231.
[6] Nunes, S. P., Ruffmann, B., Rikowski, E., Vetter, S., and Richau, R., 2002, "Inorganic Modification of Proton Conductive Polymer Membranes for Direct

Methanol Fuel Cells," J. Membr. Sci., **203**, pp. 215–225.
[7] Tominaga, Y., Hong, I., Asai, S., and Sumita, M., 2007, "Proton Conduction in Nafion Composite Membranes Filled With Mesoporous Silica," J. Power Sources, **171**, pp. 530–534.
[8] Nogami, M., Umi, Y., and Kasuga, T., 2001, "Proton Conducting Organic-Glass Composites," Fuel Cells, **1**, pp. 181–185.
[9] Ceiler, M. F., Kohl, P. A., and Bidstrup, S. A., 1995, "Plasma-Enhanced Chemical Vapor Deposition of Silicon Dioxide Deposited at Low Temperatures," J. Electrochem. Soc., **142**, pp. 2067–2071.
[10] Park, Y., and Nagai, M., 2001, "Proton Exchange Nanocomposite Membranes Based on 3–Glycidoxypropyltrimethoxysilane, Silicotungstic Acid and α-Zirconium Phosphate Hydrate," Solid State Ionics, **145**, pp. 149–160.
[11] Tung, S., and Hwang, B., 2005, "Synthesis and Characterization of Hydrated Phosphor–Silicate Glass Membrane Prepared by an Accelerated Sol–Gel Process With Water/Vapor Management," J. Mater. Chem., **15**, pp. 3532–3538.
[12] Kim, H., Prakash, S., Mustain, W., and Kohl, P. A., 2007, "Inorganic Glass Proton Exchange Membranes," *Proceedings of the 212th Meeting of the Electrochemical Society*, Washington, DC.
[13] Kim, H., Prakash, S., Mustain, W., and Kohl, P. A., 2008, "Glass-Based MEA for Micro Direct Methanol Fuel Cells," *Proceedings of the 214th Meeting of the Electrochemical Society*, Honolulu, HI.
[14] Mustain, W. E., Kim, H., Prakash, S., Stark, J., Osborn, T., and Kohl, P. A., 2007, "Platinum–Glass Composite Electrode for Fuel Cell Applications," Electrochem. Solid-State Lett., **10**, pp. B210–B213.
[15] Waszczuk, P., Wieckowski, A., Zelenay, P., Gottesfeld, S., Coutanceau, C., Léger, J., and Lamy, C., 2001, "Adsorption of CO Poison on Fuel Cell Nanoparticle Electrodes From Methanol Solutions: A Radioactive Labeling Study," J. Electroanal. Chem., **511**, pp. 55–64.
[16] Gasteiger, H. A., Markovic, N., Ross, P. N., Jr., and Calrus, E. J., 1993, "Methanol Electrooxidation on Well-Characterized Platinum-Ruthenium Bulk Alloys," J. Phys. Chem., **97**, pp. 12020–12029.
[17] Dickinson, A. J., Carrette, L. P. L., Collins, J. A., Friedrich, K. A., and Stimming, U., 2004, "Performance of Methanol Oxidation Catalysts With Varying Pt:Ru Ratio as a Function of Temperature," J. Appl. Electrochem., **34**, pp. 975–980.
[18] Mustain, W. E., Kim, H., Osborn, T., and Kohl, P. A., 2008, "Deposition of Pt_xRu_{1-x} Catalysts for Methanol Oxidation in Micro Direct Methanol Fuel Cells," Isr. J. Chem., **48**(3-4), pp. 251–257.
[19] Raghuveer, V., and Manthiram, A., 2005, "Mesoporous Carbons With Controlled Porosity as an Electrocatalytic Support for Methanol Oxidation," J. Electrochem. Soc., **152**, pp. A1504–A1510.
[20] Deivaraj, T. C., and Lee, J. Y., 2005, "Preparation of Carbon-Supported PtRu Nanoparticles for Direct Methanol Fuel Cell Applications – A Comparative Study," J. Power Sources, **142**, pp. 43–49.
[21] Leaman, F. H., 1972, "Platinum Chemical Plating," U.S. Patent No. 3,698,939.
[22] Leaman, F. H., 1972, "Deposition of Platinum by Chemical Reduction of Aqueous Solutions," Plating, **59**, pp. 440–444.
[23] Latimer, W. M., 1959, *The Oxidation States of the Elements and Their Potentials in Aqueous Solution*, 2nd ed., Prentice-Hall, Englewood Cliffs, NJ.
[24] Cotton, F. A., and Wilkinson, G., 1972, *Advanced Inorganic Chemistry: A Comprehensive Text*, 2nd ed., Wiley-Interscience, New York.
[25] Chatt, J., 1969, "Nitrogen Complexes of the Platinum Metals," Platinum Met. Rev., **13**, pp. 9–14.
[26] Rice, C., Ha, S., Masel, R. I., and Wieckowski, A., 2003, "Catalysts for Direct Formic Acid Fuel Cells," J. Power Sources, **115**, pp. 229–235.